Journal of Luminescence 173 (2016) 177–184

Contents lists available at ScienceDirect

Journal of Luminescence

journal homepage: www.elsevier.com/locate/jlumin

Full Length Article

Ln^{3+} (Ln = Ce, Tb, Dy) and Hf doping of LuI_3 powders – A material and spectroscopic study

Aneta Wiatrowska, Wilco Keur, Cees Ronda *

Philips Research, High Tech Campus 4, 5656 AE Eindhoven, The Netherlands

ARTICLE INFO

Article history:
Received 10 August 2015
Received in revised form
11 January 2016
Accepted 12 January 2016
Available online 18 January 2016

Keywords:
LuI_3:Ce
Hygroscopicity
Rare-earth elements
Luminescence
Self-trapped excitons
Scintillators

ABSTRACT

The moisture sensitivity of LuI_3:Ce,Hf and luminescent properties of undoped LuI_3 and LuI_3:M (M = Ce^{3+}, Tb^{3+}, Dy^{3+}) powders were investigated. The possibility of improving the air and moisture stability of LuI_3:Ce by Hf doping was tested. It was proven that the Hf contribution to the LuI_3:Ce stability is very limited and is insignificant to render LuI_3:Ce scintillator powders suitable for applications. Photoluminescence results of LuI_3 without dopants added on purpose showed luminescence due to a plurality of rare-earth elements' impurities. Two types of self-trapped luminescence were found. Energy transfer between host lattice, self-trapped excitons and rare-earth ions was investigated.

1. Introduction

Ce^{3+}-doped halide scintillators have been investigated extensively in the last decade in view of their high light output, excellent energy resolution, proportionality of response, short decay time and reasonably high stopping power [1–3]. The family of rare-earth halides is represented mostly by La and Lu based halides, like LaX_3 and LuX_3, where X = Cl, Br, I. $LaBr_3$:Ce and LuI_3:Ce are excellent examples of efficient halide scintillators. For this reason we investigated them in some detail.

For $LaCl_3$:Ce, apart from the Ce^{3+} doublet emission peaking at 337 and 358 nm, a shoulder associated with self-trapped emission (STE) was observed at about 400 nm. The STE emission decreases for $T > 200$ K, while opposite behavior is observed for the Ce emission. Such an anti-correlation was explained by the energy transfer towards Ce enabled by STE diffusion. Furthermore, the existence of two feeding mechanisms at Ce^{3+} sites was considered as a factor responsible for the non-exponential Ce^{3+} luminescence decay. The scintillation decay times are 24 and 44 ns with 60% contribution of the shortest component. Light output and energy resolution amount to 50,000 ph/MeV and 3.1%, respectively [4,5]. In $LaBr_3$:Ce crystals an intermediate role of STE is not relevant and fast localization of energy at Ce^{3+} results in a fast and single exponential decay (16 ns). Additionally, the higher light output, 70,000 ph/MeV, is the result of the higher number of electron–holes pairs which are generated due to the smaller band gap, compared to $LaCl_3$ [6–8]. An even smaller band gap (3.3 eV) was found for LaI_3:Ce and the small energy separation between Ce excited states and the bottom of conduction band (CB), resulting in thermal quenching, is responsible for the very poor room temperature scintillation [9]. In the series of Ce-doped Lanthanum – chloride, bromide and iodide, $LaBr_3$:Ce has the best scintillation performance.

In the case of the Lu halides, LuI_3:Ce has the highest light yield. The band gap is very small (4.52 eV), for this reason resulting in a large number of electron–hole pairs when excited with ionizing radiation. A high light output (~95,000 ph/MeV), a fast decay time (24 ns with 60% contribution) and a 3.3% energy resolution at 662 keV were reported [1,2,10,11]. However, the spectroscopic properties of this material are not yet completely understood.

Our study was motivated by the apparent possibility to decrease the moisture sensitivity of LuI_3 by co-doping with Hf [12], the observation of very efficient excitation of the emission of unintentionally doped rare-earth impurities pointing to excellent scintillation behavior and unassigned absorption and emission bands in LuI_3:Ce.

2. Synthesis

To prepare the pure iodides, Lu (4N), Ce (3N), Dy (3N), Tb (3N), Hf (2N), metals lumps or ingots were subjected to hydrogenation at 400 °C at 30 Bar in the Parr Pressure Vessel 4740. The resulting metal hydride was easily grounded to a fine powder and dehydrogenated at 700 °C in vacuum (only CeH_2 powder was

* Corresponding author.
E-mail address: cees.ronda@philips.com (C. Ronda).

http://dx.doi.org/10.1016/j.jlumin.2016.01.018
0022-2313/

dehydrogenated at 400 °C, due to the low melting point of Ce metal). The metal(s) together with a 10% molar excess of iodine were inserted into quartz ampoules that were subsequently evacuated and sealed and heated slowly (50 °C/h) using the following temperature profile: 100 °C (1 h), 150 °C (1 h), 185 °C (12 h), 230 °C (6 h), and then cooled down to room temperature [13]. The pure iodides obtained were checked with X-ray diffraction and only when they were single phase they were used in the next synthesis steps. A mixture of LuI_3 and optionally CeI_3, DyI_3, TbI_3 and/or HfI_4 was heated up to temperatures between 700 and 900 °C for 8 h in quartz ampoules, in a two-zone furnace. The temperature was limited by the reaction of the halides with quartz at 900 °C. Table 1 contains the list of synthesized compositions.

3. Experiment

LuI_3:M (M=Ce^{3+}, Tb^{3+}, Dy^{3+}, Hf^{4+}) powders are extremely air and moisture sensitive; therefore, all characterization studies were performed in gas tight cells unless mentioned differently. The phase purity of the synthesized samples was examined by powder X-ray diffraction (XRD) on a Panalytical X'Pert Pro MPD diffractometer equipped with a Cu Kα X-ray source and X'Celerator detector. The moisture stability of the synthesized powders was checked by weight measurements during constant exposure to air with around 50% humidity.

Emission and excitation spectra were recorded at room temperature using an Edinburgh Instruments Ltd. UC920 Spectrofluorometer equipped with a 450 W Xenon lamp. The moisture sensitivity was characterized by measuring the emission intensity using the same equipment under continuous irradiation with light with a wavelength of 411 nm. During this experiment powders were exposed to air with 50% humidity. For proper comparison all of them were measured on the same day. Decay measurements were performed using EPL pulsed light sources (280 nm and 375 nm) for emissions with a fast decay (Ce^{3+} emission) and with the μF920 microsecond flash lamp for emissions with a slower decay.

Table 1
Dopants concentration and firing temperature of LuI_3 synthesized powders.

%mol Ce	%mol Dy	%mol Tb	%mol Hf	Firing temperature (°C)
–	–	–	–	800
1	–	–	0–50	700–900
–	0.2–15	–	–	800
–	0.5	–	50	800
–	–	1	–	800

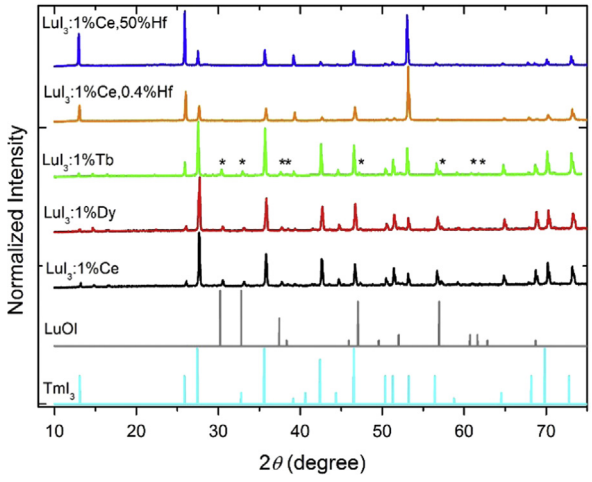

Fig. 1. X-ray diffraction patterns of LuI_3 powders singly doped with Ce, Dy, Tb and doubly doped with Ce, Hf synthesized at 800 °C and reference diffraction patterns of rhombohedral TmI_3 and hexagonal LuOI. Diffraction lines with stars (depicted for LuI_3:Tb) correspond to LuOI.

4. Structural characterization

Fig. 1 presents XRD patterns of LuI_3:1%Ce; LuI_3:1%Dy; LuI_3:1%Tb and LuI_3:1%Ce,*x*%Hf (*x*=0.4, 50) powders and reference XRD patterns of rhombohedral TmI_3 and hexagonal LuOI from a Database. Most of the XRD lines of synthesized powders are in line with the XRD pattern of rhombohedral TmI_3, as this pattern describes the rare earth iodides from SmI_3 to LuI_3. Unfortunately, a few diffraction lines (at about 30°, 33°, 38°, 47°, 57°, 61° and 62°) of the synthesized powders have been observed that do not belong to LuI_3. They rather originate from LuOI. At present, the origin of oxygen in the samples is not clear. These additional diffraction lines are appearing when Ce (1.01 Å), Dy (0.912 Å) and Tb (0.923 Å) with larger ionic radius than Lu (0.861 Å), are introduced into LuI_3 [14]. These lines are not observed for the Hf-doped samples. This is not understood.

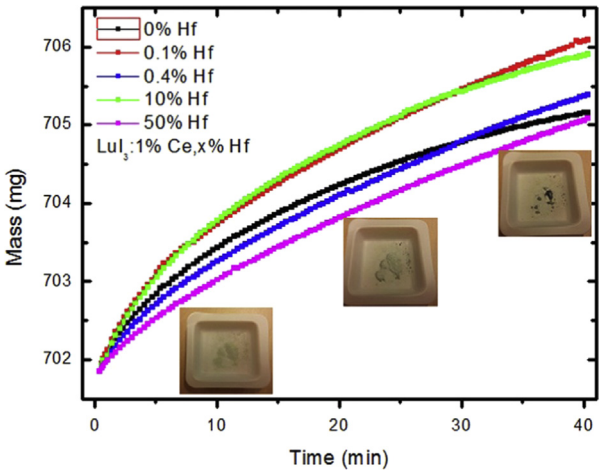

Fig. 2. Dependence of LuI_3:Ce,*x*%Hf (*x*=0–50) powders mass as a function of exposure time to air with 50% of humidity.

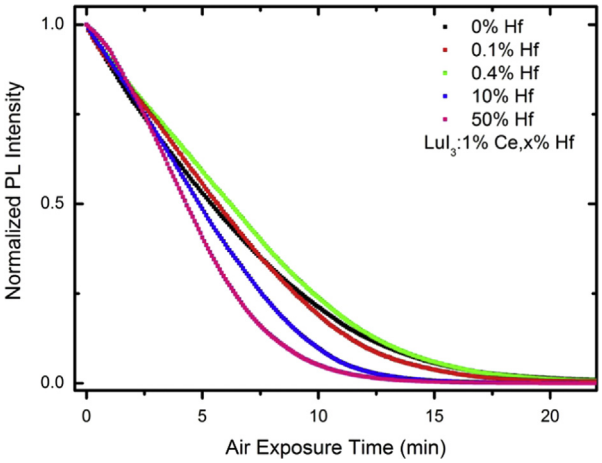

Fig. 3. Dependence of Ce^{3+}-photoluminescence intensity of LuI_3:Ce,*x*%Hf (*x*=0–50) powders as a function of air exposure time, measured during constant 411 nm irradiation.

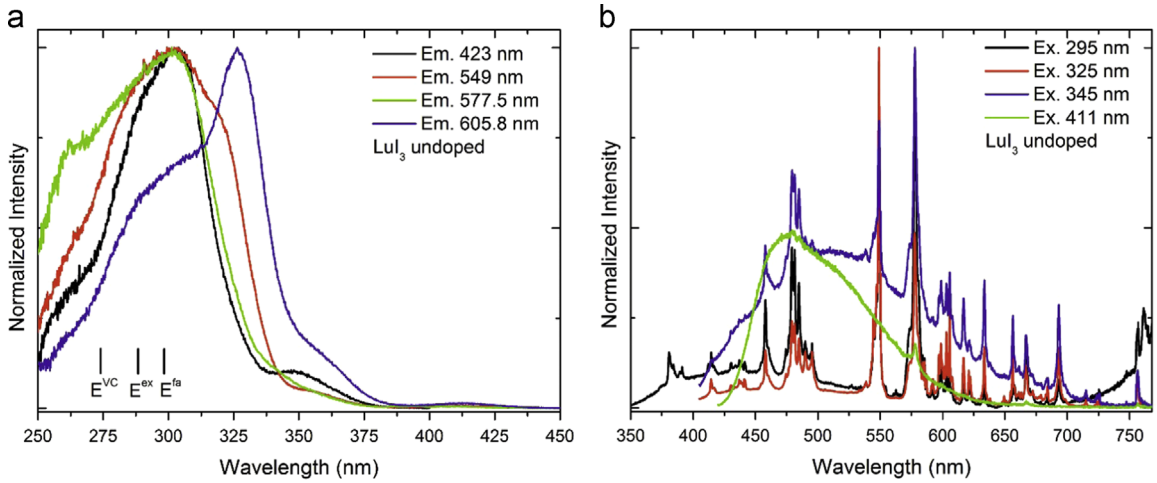

Fig. 4. Excitation spectra of different emission bands (a); emission spectra under different excitation bands (b) of unintentionally doped LuI_3 powder. (For interpretation of the references to color in this figure, the reader is referred to the web version of this article.)

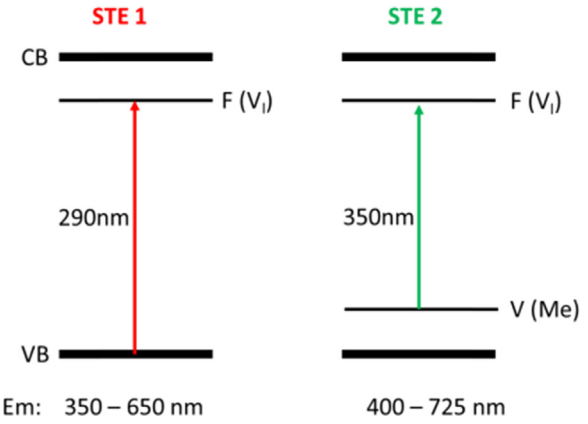

Scheme 1. The scheme of self-trapped excitons excitations and emissions occur in the range of 350–650 nm (STE 1) and 400–725 nm (STE 2) respectively.

4.1. LuI_3:Ce,Hf

The most known and the most challenging issue of LuI_3:Ce: its air and moisture sensitivity was investigated by Vyprintsev in [12]. This author investigated Hf co-doping (0.05–1.5 mol%), added as HfI_4, as a way to obtain non-hygroscopic cerium activated lutetium iodide monocrystals. The composition $Lu_{0.986}Hf_{0.004}Ce_{0.01}I_{3.004}$ was found to be non-hygroscopic as the surface of the single crystals did not change after 4 h exposure to air with about 50% relative humidity and the luminescence light yield after exposure was still 96% [12]. We have examined this phenomenon for powders. LuI_3:1%Ce co-doped with Hf (0.1–50 mol%) powders were synthesized in the way as described in Section 2.

Fig. 2 shows the increase of the mass of the LuI_3:Ce powders co-doped with different concentrations of Hf powders as a function of air exposure time. During the first 30 min, the weight of powders co-doped with 0.4% and 50% of Hf samples increased more slowly than for LuI_3:Ce. The weight increased rapidly for powders with 0.1% and 10% of Hf. The lowest weight increase was exhibited by LuI_3:1%Ce,50%Hf powder. However, after 40 min exposure time all powders showed deliquescence independent of the Hf content. Fig. 3 presents kinetic scans (monitoring of 475 nm luminescence intensity as a function of time) measured under constant irradiation with light with wavelength 411 nm in air. The photoluminescence intensity decreases with air exposure time for all samples, slightly dependent of the Hf content. The most rapid drop is observed for sample doped with 50% of Hf. This result is the opposite as expected, based on the weight experiments. Only the sample with 0.4% Hf shows slightly better properties than the undoped LuI_3:Ce powder. Despite that, after 20 min no luminescence is observed anymore for any of the samples. All samples are still very water sensitive despite the fact that they were codoped with Hf. The differences may be due to differences in grain size: they are not related to the Hf-content. We have not investigated this in more detail in view of the very minor effects encountered on co-doping with Hf.

5. Spectroscopy of unintentionally doped LuI_3 and LuI_3 doped with Ce, Tb and Dy

5.1. Unintentionally doped LuI_3

Fig. 4a shows excitation spectra of the 423, 549, 577.5 and 605.8 nm emissions, related to self-trapped excitons (STE), 4f–4f Tb^{3+}, 4f–4f Dy^{3+} and 4f–4f Pr^{3+} luminescence, respectively. The energies of the onset of the fundamental absorption (band to band, E^{fa}), the exciton creation peak (E^{ex}) and the edge of conduction band (E^{VC}) of LuI_3 host were already reported by Birowosuto et al. and Srivastava [11,15] and occur at 4.15 eV (298 nm), 4.30 eV (288 nm) and 4.53 eV (274 nm), respectively (Fig. 4a).

The excitation spectrum of the STE emission located at 423 nm has two main broad bands related to the host lattice. These bands are peaking at 290 and 350 nm (Fig. 4a, Scheme 1).

The excitation spectrum of Tb emission ($\lambda_{em}=549$ nm) (Fig. 4a) besides host lattice related band (300 nm) also has a band with maximum at 320 nm, which is assigned to a 4f–5d Tb^{3+} transition, see also [16].

The excitation spectrum of Dy luminescence (577.5 nm) has a very broad, nonsymmetric band with three main peaks at around 260, 300 and 350 nm of which the intensity increases in the UV region of the spectra (Fig. 4a).

Four broad excitation bands peaking at 300, 325, 360 and 410 nm are observed in the excitation spectrum of Pr^{3+} emission (605.8 nm); these bands are connected to the host lattice, and to Pr^{3+} and Ce^{3+} (Fig. 4a). Srivastava [15] investigated the $I^- \rightarrow Pr^{3+}$ charge transfer transition in LuI_3:Pr samples. The CT $I^- \rightarrow Pr^{3+}$ is associated with a broad excitation band peaking at 325 nm and corresponds to an electron transfer from the top of valence band (I

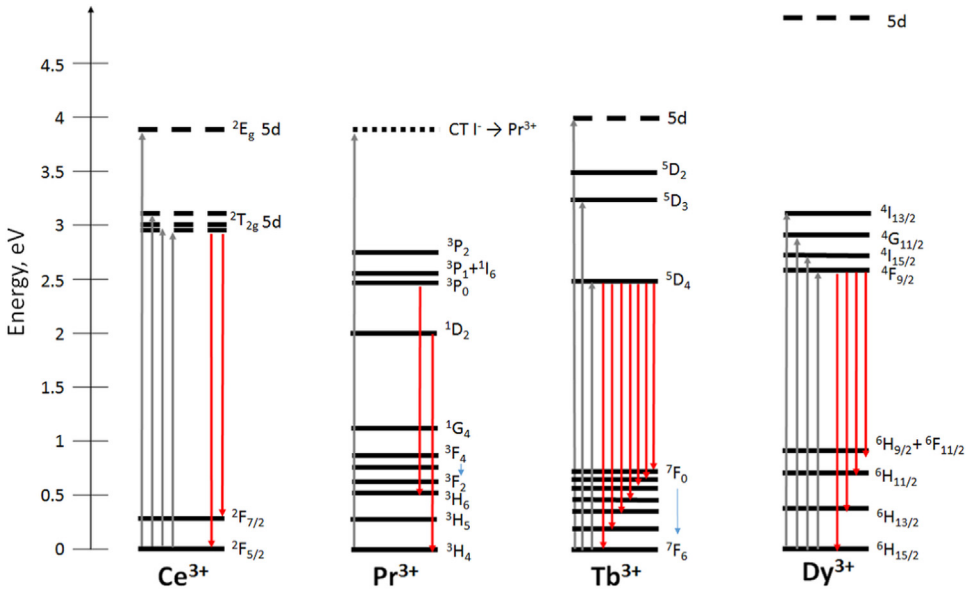

Scheme 2. Schematic diagram of the Ce^{3+}, Pr^{3+}, Tb^{3+} and Dy^{3+} energy levels and transitions occurring in LuI_3 contaminated by these rare-earth ions.

Table 2
The positions of Ce^{3+}, Pr^{3+}, Tb^{3+}, and Dy^{3+} ion transitions of unintentionally doped LuI_3. Data summarized in the table were presented in Fig. 4b and Scheme 2. Crystal field interactions may lead to more lines than depicted in this scheme.

Ln^{3+}	Transition	Range (nm)	Range (eV)
Emission spectra			
Ce	5d 4f	420–675	1.84–2.95
Pr	$^1D_2$–$^3H_4$	590–610	2.03–2.10
	$^3P_0$–$^3H_6$	633	1.96
Tb	$^5D_4$–$^7F_{J\ (J=6-0)}$	465–504; 530–558;	2.46–2.67; 2.22–2.34
		580–610; 614–636;	2.03–2.14; 1.95–2.02
		643–660; 665–675;	1.88–1.93; 1.84–1.86
		680–685	1.81–1.82
Dy	$^4F_{9/2}$–$^6H_{15/2}$	450–490	2.53–2.76
	$^4F_{9/2}$–$^6H_{13/2}$	570–590	2.10–2.18
	$^4F_{9/2}$–$^6H_{11/2}$	650–675	1.91–1.84
	$^4F_{9/2}$–$^6F_{11/2}$+$^6H_{9/2}$	753–760	1.63–1.65

p-orbitals) to the Pr^{3+} ion. This is in line with the Dorenbos model [16]. It implies Pr^{2+} to be formed in this excited state.

The 290 nm absorption is thought to be due to the transition of electrons from the valence band (VB) to I-vacancies not occupied with an electron; this would place the F-center (I-vacancy) about 1 eV below the conduction band (CB). The emission peaking at 440 nm can very well be due to STE formation (STE1), the F-center (that has captured an electron) localizing the hole in the CB, leading to significant lattice relaxation and consequently in a significant Stokes Shift.

The occurrence of 350 nm absorption band in LuI_3:Ce was reported by Birowosuto [11] and in LuI_3:Pr by Srivastava [15]; its origin is not understood. Birowosuto observed a decrease in the intensity of this band on increasing Ce^{3+} concentration at room temperature [11]. As argued by Srivastava [15], this excitation band is very likely due to host lattice states. It is not due to Ce^{3+}, as its intensity decreases on increasing Ce^{3+} concentration, also at low Ce^{3+} concentration, very likely excluding concentration quenching on Ce^{3+} and rather pointing to energy transfer to Ce^{3+}, see [15]. At low temperatures, excitation in this band yields broad band emission, peaking at 540 nm [15]. We propose that the absorption at about 350 nm is due to the transition from electrons on metal ion vacancies ($V_{(Me)}$) to I-vacancies. As a result, the metal ion vacancy is located about 0.8 eV above the VB.

In the series of Lanthanides, only in the case of Pr^{3+} emission we see a well expressed excitation band peaking at some 350 nm (Fig. 4a, violet line). We assume that the same band is also observed in the excitation spectrum of the STE emission (Fig. 4a, black line). This may be related to a more efficient energy transfer from STE states to Pr^{3+} than to Tb^{3+}or Dy^{3+}, as only in case of Pr^{3+}, spin allowed transitions are encountered in the energy range where STE emission is observed. Please also note the absence of sharp lines in the excitation spectra of undoped LuI_3 (independent of the emission monitored) in the spectral range 375–450 nm.

Fig. 4b presents emission spectra under 295, 325, 345 and 411 nm excitations of unintentionally doped LuI_3 powder. The emission lines observed can be assigned to Tb^{3+}, $Dy^{3+}$and Pr^{3+}. Based on luminescence spectra of unintentionally doped LuI_3, Scheme 2 and Table 2 were constructed. They present positions of energy levels of selected Lanthanides and transitions observed in LuI_3.

Additionally, three ranges of broad band luminescence types: 350–650 nm, 400–750 nm and 425–700 nm, registered under 295 or 325 nm, 345 nm and 411 nm excitation respectively, can be clearly distinguished (Fig. 4b). They are related to 2 types of emissions. The first two bands are considered to be self-trapped exciton emissions (STE 1 and STE 2). The band peaking at 475 nm is due to the Ce^{3+} 5d–4f transition.

The emission band peaking at 540 nm can very well be due to STE formation (STE2) consisting of the F-center (that has captured an electron) and a hole on the metal ion vacancy. We expect a very large lattice relaxation in view of the fact that the electric charge on both defects changes as a consequence of the optical transition. Therefore, at higher temperatures, the strong lattice relaxation likely results in thermal quenching of the STE emission, as has been reported by Srivastava [15]. Thermal quenching may be due to a thermally activated mobility increase of the STE to centers for non-radiative recombination or alternatively direct recombination of electron and hole due to crossing of ground and excited state potential energy parabolas at relatively low potential energy in the excited state. Promotion of charges from defect states to the conduction or valence band would also lead to quenching of the STE emissions. We do not think these processes to cause thermal quenching: the estimated trap depths are relatively high whereas quenching already sets in well below 300 K [11].

We now try to correlate this model to the observation of a difference in luminescence quenching behavior when LuI_3:Ce is excited with X-ray radiation and UV radiation (absorption on Ce^{3+}), as reported in Ref. [11]. It was observed that thermal quenching sets in at lower temperatures already when exciting using X-ray radiation. At elevated temperatures, thermal quenching of the STE emissions will result in considerably increased non-radiative recombination rates, and this may lead to efficient quenching of the scintillation emission also, by a reduced feeding of the Ce^{3+} excited states.

LuI_3:Ce is an efficient scintillator, so efficient energy transfer from STE to Ce^{3+} is desired. We see huge spectral overlapping between the STE emission and Ce absorption, which means that energy transfer is rather likely to happen. Fortunately, energy transfer from Ce^{3+} to STE states is not very likely, in view of the absence of spectral overlap between the Ce^{3+} emission and STE absorption bands.

The emission spectrum (Fig. 4b) of unintentionally doped LuI_3 shows line emissions due to a number of 4f elements. In the excitation spectra, no lines are observed. This shows that the concentration of the rare-earth impurities is rather small and that energy transfer from host lattice states to these rare-earth impurities very likely is very efficient. This is a prerequisite for efficient scintillation.

Monoexponential decay curves were measured for the 549 nm, 577.5 nm, and 633 nm emissions corresponding to emissions originating from Tb^{3+}, Dy^{3+} and Pr^{3+} ions respectively and it was found that Tb and Dy luminescence decay times from undoped sample both are in line with their decay times for LuI_3:Tb and LuI_3:Dy respectively (Fig. 5 compared with Figs. 9 and 11). The decay times found were 910 μs (Tb), 355 μs (Dy) and 19 μs (Pr). A similar value for the Pr^{3+} emission decay time was already reported for oxygen free compounds, like KYF_4:Pr [17]. Our finding confirms that the unintentionally doped sample is contaminated by Pr as well, and the absorption band peaking at 325 nm very likely originates from a charge transfer transition involving the valence band.

We did not observe a slow component in the emission of Pr^{3+}, Tb^{3+}, and Dy^{3+}, as was observed in case of Ce^{3+} doped materials. This is understandable as the emission originating from Pr, Tb, and Dy is much slower than even the slowest component of the Ce^{3+} emission.

In case of emissions at 549 nm (Tb) and 577 nm (Dy), we see a very fast initial decay. This is assigned to Ce^{3+} emission, the time of dependence of which is governed by the time stamp of the flash lamp, as the Ce^{3+} emission intensity decreases much faster than the lamp intensity as a function of time after the flash. The larger the wavelength (for wavelengths above 475 nm), the smaller the

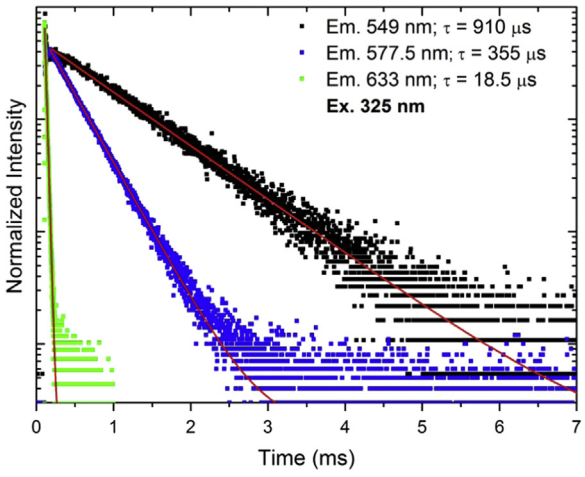

Fig. 5. Decay curves of 549, 577.5 and 633 nm emissions of undoped LuI_3 under 325 nm excitation.

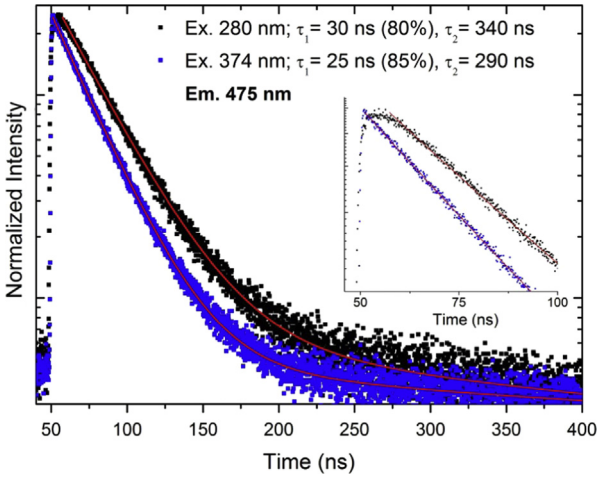

Fig. 7. Decay curves of 475 nm emission of LuI_3:1% Ce under 280 and 374 nm excitations. Inset: enlarged decay curves.

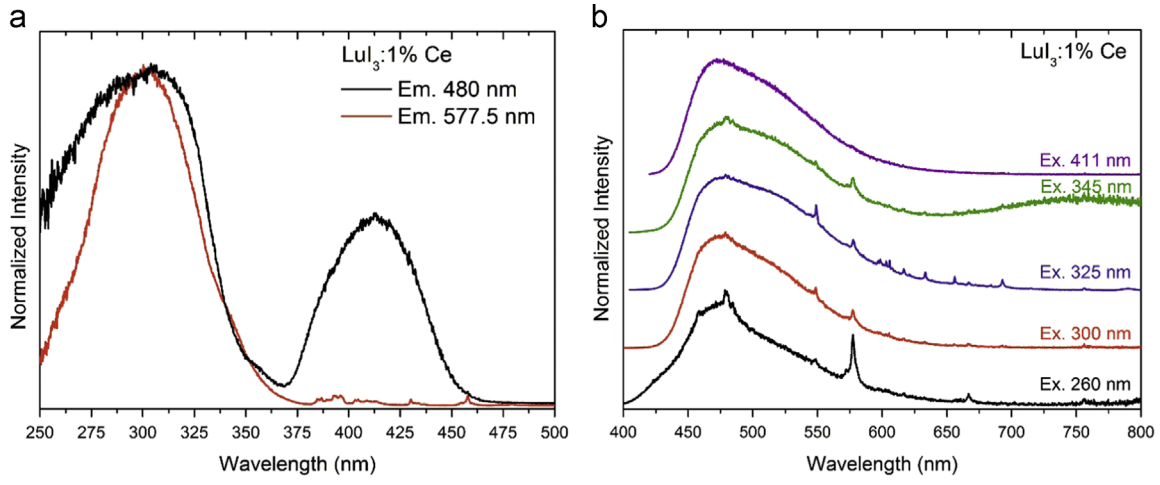

Fig. 6. Excitation spectra of 480 nm and 577.5 nm emissions (a) and emission spectra under 260 nm, 300 nm, 325 nm, 345 nm and 411 nm excitations (b) of LuI_3:1%Ce powder.

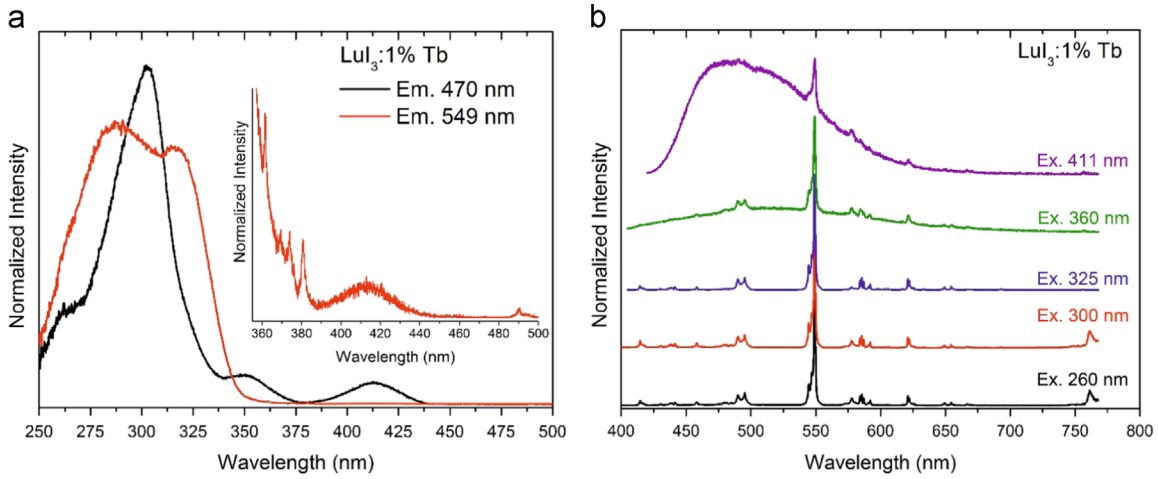

Fig. 8. Excitation spectra of 470 and 549 nm emissions (a); emission spectra under 260 nm, 300 nm, 325 nm, 360 nm and 411 nm excitations (b) of LuI_3:1% Tb powder. Inset: enlarge excitation spectrum of 549 nm emission. (For interpretation of the references to color in this figure, the reader is referred to the web version of this article.

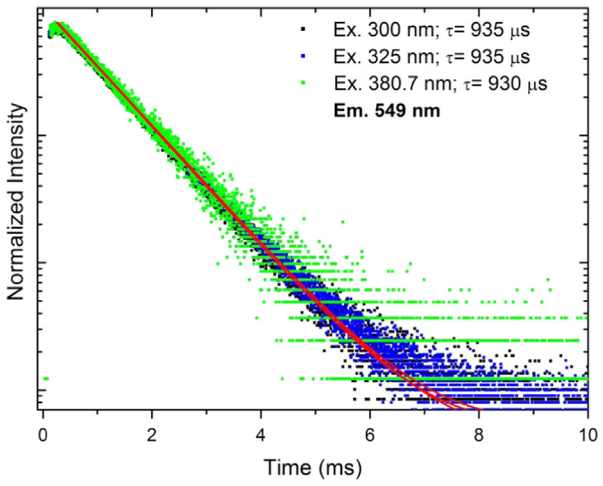

Fig. 9. Decay curves of 549 nm emission of LuI_3:1%Tb under 300, 325 and 380.7 nm excitations.

contribution of the Ce^{3+} emission to the fast initial decay is expected to be. For this reason, we do not see fast initial decay in case of Pr^{3+} emission at 633 nm.

5.2. LuI_3:Ce

The Ce^{3+} $4f^1$ ground state configuration generates two levels $^2F_{5/2}$ and $^2F_{7/2}$, separated by some 2000 cm^{-1} because of spin orbit coupling. The $5d^1$ configuration is split by the crystal field into 2–5 components with a total splitting up to some 15,000 cm^{-1}.

Usually, the Ce^{3+} luminescence has a double band shape and appears in the UV or blue spectral region, although it can e.g. also be observed in the yellow spectral region when the ligand field strength or the covalent character of the chemical bonding is large, this is f.e. encountered in garnets, see f.e. [18] for a recent review.

Fig. 6a shows excitation spectra of different emissions of LuI_3:1%Ce powders. The broad excitation band peaking at 300 nm is due to LuI_3 host lattice absorption. On the low energy side of this broad band we can distinguish an additional band in the range of 343–368 nm. The same band seems to be present for undoped samples but then it is much broader, up to 384 nm (Fig. 4a). At 384 nm, Ce^{3+} is already excited directly, with relatively high intensity (comparison Figs. 4a and 6a), obscuring the weak excitation in this spectral range which is not due to Ce^{3+} absorption. The band peaking at 410 nm is due to 4f–5d Ce^{3+} transitions. Dorenbos showed that in this region three excitation bands at 396, 414 and 420 nm are present [11] (see Scheme 2).

The emission spectrum of LuI_3:Ce presents typical Ce luminescence: two overlapping bands, in this case at 475 and 525 nm (Fig. 6b). Contamination emission related to Dy^{3+} (577.5 nm) and Tb^{3+} (549 nm) is very well seen under host lattice excitation. However, no or hardly any luminescence due to impurities or STEs is visible under direct Ce^{3+} (411 nm) excitation (a trace of Dy^{3+} emission may be visible at 577 nm). This implies that there is no efficient energy transfer from Ce^{3+} to impurities (Fig. 6b). This may be due to the relatively low Ce^{3+} concentration. Under 260 nm excitation overlap of STE1 emission (high energy side) and Ce luminescence is observed (Fig. 6b), indicating that STE1 is mobile.

Decay curves of Ce^{3+} luminescence (λ_{em}=475 nm, λ_{ex}=280 or 374 nm) for LuI_3:Ce powder are presented in Fig. 7. The decay curves excited via the host (280 nm) can be fitted using two components: a slow one with a decay time around 340 ns and a faster one with a decay time around 30 ns. On direct Ce excitation (374 nm), similar values are obtained. The fast component of the Ce emission is connected to the generation of electron–hole pairs on Ce^{3+} and the slow component with electron and/or hole trapping and delayed excitation of Ce^{3+}. Energy transfer from host lattice states to Ce is confirmed by the decay rise registered under 280 nm excitation (Fig. 7 inset). The observation of a slow component in the Ce-emission on excitation into Ce implies that ionization of Ce^{3+} to Ce^{4+} occurs in the excited state.

5.3. LuI_3:Tb

The first spin allowed transition 4f–5d Tb^{3+} is expected at (1.66 ± 0.12 eV) higher energy than the 4f–5d transition with the highest energy in Ce^{3+} [16]. We therefore predict to see the first spin allowed 4f–5f Tb transition in LuI_3 at about 270 nm. Based on Hund's rule, the spin forbidden transition is located at lower energy and is expected at (0.7 ± 0.05 eV) lower energy than the first spin allowed transition [19], i.e. about 316 nm.

Fig. 8a shows excitation spectra of the 470 nm (5d–4f Ce^{3+}) and 549 nm (4f–4f Tb^{3+}) emissions. Please note that Ce is an unintentionally introduced impurity. The excitation spectrum of the 549 nm emission (red line) consists of two broad bands peaking at around 280 nm and 320 nm corresponding to host lattice and 4f–5d absorption of Tb^{3+}, respectively. The 4f–5d spin forbidden transition position of Tb^{3+} is in line with Dorenbos'

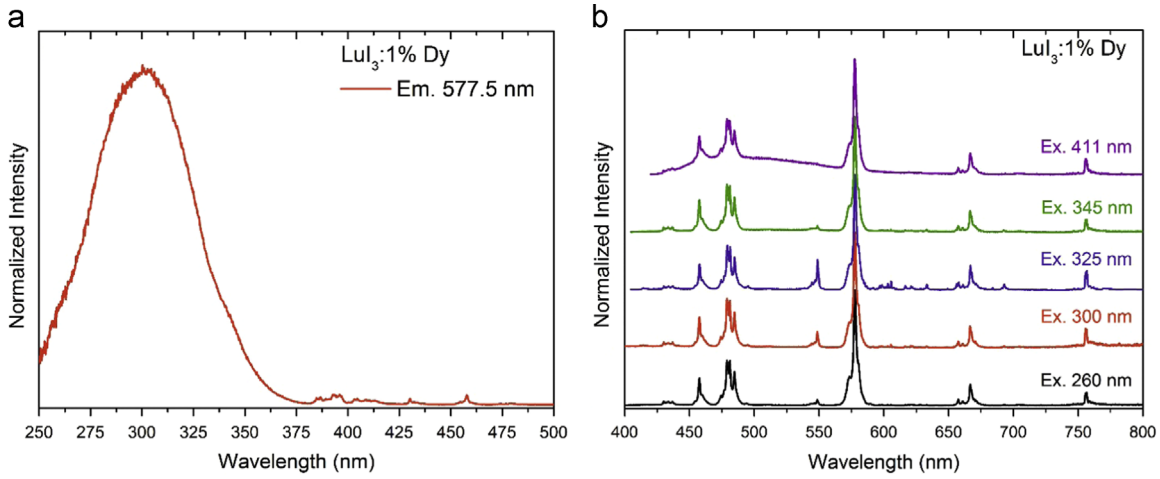

Fig. 10. Excitation spectrum of 577.5 nm emission (a) and emission spectra under 260 nm, 300 nm, 325 nm, 345 nm and 411 nm excitations (b) of LuI_3:1%Dy powder.

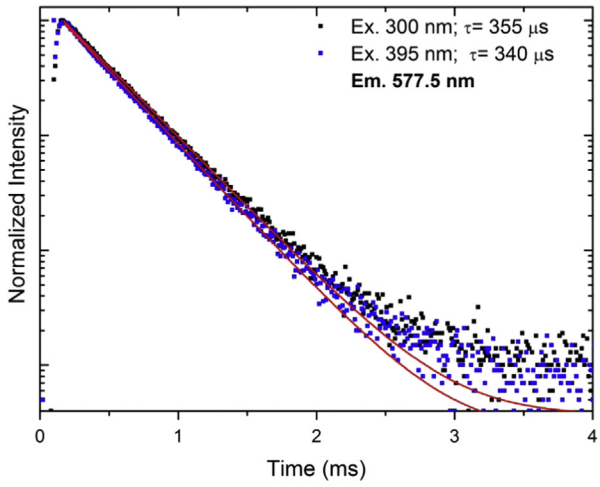

Fig. 11. Decay curves of 577.5 nm emission of LuI_3:1%Dy under 300 and 395 nm excitations.

predictions [16], see above also. The spin allowed optical transition on Tb^{3+} (expected at about 316 nm) was not observed: it coincides with the host lattice absorption. The excitation spectrum above 350 nm is composed of 4f–4f transition of Tb^{3+} ion (peaks appear at 361, 379, 374, 380 and 490 nm) and a 4f–5d transition of Ce^{3+} (broad band peaking at around 410 nm) (see Fig. 8a, inset). The STE 2 excitation band peaking at 350 nm appears only when 470 nm emission is monitored. In case of the undoped LuI_3 sample, at this emission wavelength, overlap of STE emissions (STE 1 and STE 2) and Ce^{3+} luminescence occurs (please compare Fig. 4b with Fig. 8b).

Emission spectra under different excitations are shown in Fig. 8b. Under 260, 300 and 325 nm excitations we can observe pure Tb^{3+} luminescence with peaks in the ranges of 465–504 nm, 530–558 nm, 580–610 nm, 614–636 nm, 643–660 nm, 665–675 nm and 680–685 nm connected to $^5D_4$–^7F_J (J=6–0) transitions of Tb^{3+}. We also observed low intensity emission lines originating from Pr^{3+} contamination: 606 and 633 nm. They are assigned to $^1D_2$–$^3H_4$ and $^3P_0$–$^3H_6$ transitions (see Table 2 and Scheme 2).

Under 411 nm excitation, Ce luminescence peaking at 480 nm shows overlap with Tb emission with the most intense peak at 549 nm being observed (Fig. 8b). The existence of both Ce^{3+} and Tb^{3+} luminescence proves the occurrence of efficient energy transfer from Ce^{3+} to Tb^{3+}: Tb^{3+} shows no absorption at this wavelength (411 nm).

Under 360 nm, besides Tb emission lines, a very broad band in the range of 400–675 nm appeared (Fig. 8b). This STE emission (STE2) was already observed for unintentionally doped LuI_3 (Fig. 4b). In this case , the coexistence of both Tb^{3+} and STE2 emission proves mixed excitation, please note that Tb^{3+} to STE2 energy transfer is excluded as excitation of Tb^{3+} at shorter wavelengths does not result in STE2 emission. The excitation spectra show 4f–4f Tb excitation lines and the STE 2 broad excitation band at 360 nm (Fig. 8a).

The 4f–4f Tb^{3+} luminescence was found under 325 nm excitation and no energy transfer from Tb to Ce, and from Tb to STE was observed (Fig. 8b). Even under host-lattice excitation (under 300 nm) only Tb emission was seen. This likely is due to the very low Ce^{3+} impurity concentration as LuI_3:Ce is a very efficient scintillator.

Fig. 9 presents decay curves of Tb luminescence (549 nm) recorded under host lattice excitation (300 nm), 4f–5d Tb^{3+} excitation (325 nm) and 4f–4f Tb^{3+} excitation (380.7 nm). Independent of the excitation wavelength, the same decay times were obtained for LuI_3:1%Tb powder (Fig. 9). They can be fitted by monoexponential curves with a decay time around 930 μs. Decay times in the order of 1 ms are frequently observed for Tb^{3+} emissions. The value obtained implies that the quantum efficiency of the emission is rather high: close to unity.

5.4. LuI_3:Dy

The first spin allowed Dy^{3+} 4f–5d transition is expected to be 3.11 ± 0.07 eV higher energy than the first 4f–5d transition in Ce^{3+} [16]. We therefore expect this band around 205 nm. As a consequence, the Dy^{3+} first spin forbidden transition, which is located at a 0.64 eV lower energy than first spin allowed transition, is expected around 228 nm, see Ref. [16]. The second Dy^{3+} spin forbidden 4f–5d transition is expected at 0.91 eV lower energy than first spin allowed transition. We expect this band around 240 nm.

The emission of Dy^{3+} in LuI_3 consists of two dominant bands. The blue emission band ($^4F_{9/2}$–$^6H_{15/2}$ transition) is assigned to a magnetic dipole transition, the intensity of which hardly varies with variations in the crystal field. The yellow emission band (transition $^4F_{9/2}$–$^6H_{13/2}$) is a hypersensitive transition which has ΔJ=2 (electric dipole transition) and is allowed only in the absence of an inversion center. Consequently, when the Dy^{3+} ion is located at a low symmetry site, the yellow emission dominates in luminescence spectrum. In contrast, when the Dy^{3+} ion occupies a high symmetry site, the blue emission is stronger [20–22].

The Dy^{3+} excitation spectrum consists of the host lattice broad band peaking at 300 nm and sharp lines located at 385–415 nm, 428–440 nm and 450–468 nm, corresponding to $^6H_{15/2}$–$^4I_{13/2}$, $^6H_{15/2}$–$^4G_{11/2}$ and $^6H_{15/2}$–$^4I_{15/2}$ transitions of Dy^{3+}, respectively (Fig. 10a). An additional band at 350 nm is also observed and its origin was already discussed in a previous section.

The emission spectra mostly show sharp peaks located in the range of 450–490 nm, 570–590 nm, 650–675 nm and 753–760 nm, corresponding to $^4F_{9/2}$–$^6H_{15/2}$, $^4F_{9/2}$–$^6H_{13/2}$, $^4F_{9/2}$–$^6H_{11/2}$, $^4F_{9/2}$–$^6F_{11/2}+^6H_{9/2}$ transitions of Dy^{3+}, respectively (Fig. 10b). However, under host lattice excitation (from 260 to 345 nm) we also observed Tb^{3+} luminescence (549 nm peak) with the highest intensity under 325 nm. In Section ,5.3 it was mentioned that the spin forbidden transition of Tb^{3+} is expected in the range of 306–327 nm and it confirms the more intense Tb emission under 325 nm excitation. However Tb^{3+} is not the only one undesired contamination seen under 325 nm excitation. Red Pr^{3+} luminescence around 606 and 630 nm was observed also under 325 nm excitation. It confirms Srivastava's assumption [15] that the 325 nm excitation band finds its origin in the $I^- \rightarrow Pr^{3+}$ charge transfer transition. The same behavior was observed also for LuI_3:Ce sample (Fig. 6b).

Under 411 nm excitation, the broad band luminescence connected to the Ce contamination was observed. Please note the very weak absorption centered around 400 nm that may be due to Ce^{3+}. We anticipate Ce–Dy energy transfer as under 411 nm excitation we observe both Ce^{3+} and Dy^{3+} emission. Only in case of excitation with 411 nm radiation, no trace of Tb^{3+} emission was observed at 549 nm. This indicates, if at all, only a rather weak Dy–Tb or Ce–Tb energy transfer. This may be due to the very low impurity concentrations. It may also indicate that the host lattice to Tb^{3+} energy transfer is much stronger than the host lattice to Dy^{3+} energy transfer. This implies that we do not expect LuI_3:Dy to be a very good scintillator.

Decay traces of Dy luminescence in LuI_3:Dy were measured under 395 nm ($^6H_{15/2}$–$^4I_{13/2}$ Dy^{3+} transition) and 300 nm excitations (host lattice) (Fig. 11). The decay curves can be moderately successfully fitted with a monoexponential curve. Independent on the excitation wavelength the decay times are very similar, around 350 μs. Such an emission decay time is encountered for Dy^{3+} quite frequently.

6. Conclusions

LuI_3 powders were synthesized from the elements (viz. Lu metal and I_2). Hf-co-doped LuI_3:Ce powders were checked for their moisture stability. Unfortunately, no positive effect of Hf doping on LuI_3:Ce hygroscopicity was found, independent on the Hf concentration in contrast to a report in the literature [12].

Spectroscopic investigations have shown that undesired contaminations coming from Lu metal are present in unintentionally doped LuI_3 samples. In-depth analysis allows to characterize the luminescence properties of Ce^{3+}, Tb^{3+}, Dy^{3+} and Pr^{3+} in LuI_3. In addition, two STE excitation and emission bands are reported and their origin discussed. Energy transfer from these STEs to Ce^{3+} could be observed as a consequence of spectral overlap between Ce^{3+} absorption band and the STE 1 and 2 emission bands.

Acknowledgments

The presented work was supported by European Union through the Marie Curie Initial Training Network LUMINET, Grant agreement no. 316906.

References

[1] K.S. Shah, J. Glodo, M. Klugerman, W. Higgins, T. Gupta, P. Wong, W.W. Moses, S.E. Derenzo, M.J. Weber, P. Dorenbos, IEEE Trans. Nucl. Sci. 51 (2004) 2302.
[2] M.D. Birowosuto, P. Dorenbos, C.W.E. van Eijk, K.W. Krämer, H.U. Güdel, J. Appl. Phys. 99 (2006) 123520-1.
[3] E.V.D. van Loef, P. Dorenbos, C.W.E. van Eijk, K.W. Krämer, H.U. Güdel, Nucl. Instrum. Methods Phys. Res. A 496 (2003) 138.
[4] E.V.D. van Loef, P. Dorenbos, C.W.E. van Eijk, K.W. Krämer, H.U. Güdel, IEEE Trans. Nucl. Sci. 48 (2001) 341.
[5] E.V.D. van Loef, P. Dorenbos, C.W.E. van Eijk, J. Phys. Condens. Matter 15 (2003) 1367.
[6] E.V.D. van Loef, P. Dorenbos, C.W.E. van Eijk, Appl. Phys. Lett. 79 (2001) 1573.
[7] E.V.D. van Loef, P. Dorenbos, C.W.E. van Eijk, K.W. Krämer, H.U. Güdel, Nucl. Instrum. Methods Phys. Res. A 486 (2002) 254.
[8] P. Dorenbos, E.V.D. van Loef, A.P. Vink, E. van der Kolk, C.W.E. van Eijk, K. W. Krämer, H.U. Güdel, W.M. Higgins, K.S. Shah, J. Lumin. 117 (2006) 147.
[9] A. Bessiere, P. Dorenbos, C.W.E. van Eijk, K.W. Krämer, H.U. Güdel, C. de Mello Donega, A. Meijerink, Nucl. Instrum. Methods Phys. Res. A 537 (2005) 22.
[10] K.W. Krämer, P. Dorenbos, H.U. Güdel, C.W.E. van Eijk, J. Mater. Chem. 16 (2006) 2773.
[11] M.D. Birowosuto, P. Dorenbos, J.T.M. de Haas, C.W.E. van Eijk, K.W. Krämer, H. U. Güdel, J. Lumin. 118 (2006) 308.
[12] D.I. Vyprintsev, Inorganic Scintillating Material, Crystal Scintillator and Radiation Detector, U.S. Patent 2012305779, December 6, 2012.
[13] G. Meyer, L.R. Morss, Synthesis of Lanthanide and Actinide Compounds, Kluwer Academic Publishers, The Netherlands, 1990.
[14] R.D. Shannon, Acta Crystallogr. A 32 (1976) 751.
[15] A.M. Srivastava, Opt. Mater. 30 (2008) 1567.
[16] P. Dorenbos, J. Lumin. 91 (2000) 155.
[17] Z. Xia, A. Arcangeli, R. Faoro, M. Tonelli, Optoelectron. Adv. Mater. 5 (2011) 336.
[18] C. Ronda, Prog. Electromagn. Res. 147 (2014) 81.
[19] R.T. Wegh, A. Meijerink, Phys. Rev. B 60 (1999) 10820.
[20] W.Y. Shen, M.L. Pang, J. Lin, J.J. Fang, Electrochem. Soc. 152 (2005) H25.
[21] Q. Su, H. Liang, C. Li, H. He, Y. Lu, J. Li, Y. Tao, J. Lumin. 122 (2007) 927.
[22] K. Mini Krishna, G. Anoop, M.K. Jayaraj, Electrochem. Soc. 154 (2007) J310.